

**This is the accepted manuscript version of the contribution published as:**

Guo, W., Huang, S., Huang, Q., Leng, G., Mu, Z., Han, Z., Wei, X., She, D., Wang, H., Wang, Z., **Peng, J.** (2023):  
Drought trigger thresholds for different levels of vegetation loss in China and their dynamics  
*Agric. For. Meteorol.* **331** , art. 109349

**The publisher's version is available at:**

<http://dx.doi.org/10.1016/j.agrformet.2023.109349>

# **Drought trigger thresholds for different levels of vegetation loss in China and their dynamics**

**Wenwen Guo<sup>a</sup>, Shengzhi Huang<sup>a\*</sup>, Qiang Huang<sup>a</sup>, Guoyong Leng<sup>b</sup>, Zhenxia Mu<sup>c</sup>,  
Zhiming Han<sup>a</sup>, Xiaoting Wei<sup>a</sup>, Dunxian She<sup>d</sup>, Hanye Wang<sup>a</sup>, Zhixia Wang<sup>a</sup>, and Jian  
Peng<sup>e,f</sup>**

- a. State Key Laboratory of Eco-Hydraulics in Northwest Arid Region of China, Xi'an University of Technology, Xi'an 710048, China
- b. Key Laboratory of Water Cycle and Related Land Surface Processes, Institute of Geographic Sciences and Natural Resources Research, Chinese Academy of Sciences, Beijing 100101, China
- c. Xinjiang Key Laboratory of Hydraulic Engineering Security and Water Disasters Prevention, Urumqi 830052, Xinjiang, China
- d. State Key Laboratory of Water Resources and Hydropower Engineering Science, Wuhan University, Wuhan 430072, China
- e. Department of Remote Sensing, Helmholtz Centre for Environmental Research–UFZ, Permoserstrasse 15, 04318 Leipzig, Germany
- f. Remote Sensing Centre for Earth System Research, Leipzig University, 04103 Leipzig, Germany

---

\* Corresponding author at: State Key Laboratory of Eco-hydraulics in Northwest Arid Region of China, Xi'an University of Technology, Xi'an 710048, China. Tel.: +86 29 82312801; fax: +86 29 82312797. E-mail Address: [huangshengzhi7788@126.com](mailto:huangshengzhi7788@126.com).

**Abstract:** Frequent meteorological droughts can negatively impact terrestrial ecosystems by controlling the opening and closing of vegetation stomatal and altering vegetation structure to limit the ability of vegetation to sequester carbon. Due to the lagging and accumulation effects of drought on vegetation growth, drought trigger thresholds for different levels of vegetation loss are still unclear, which is very important for accurately assessing the future impacts of drought on terrestrial ecosystem. Therefore, this study proposed a framework to investigate drought trigger thresholds under various vegetation losses based on copula theory and conditional probabilities, and assessed the dynamics of drought trigger thresholds and possible causes, based on the random forest model. In addition, we used multiple GPP and soil water datasets for the analysis to ensure the robustness of relevant findings. The results show that: (1) there is a generally positive correlation between GPP and SPEI in China, and the response time of vegetation to drought is mostly on a short time scale (less than or equal to 4 months); (2) drought trigger thresholds are also higher in eastern China, with lower vegetation resistance and significantly higher risk of vegetation productivity loss than in other regions; (3) the trigger thresholds in northeastern China show a decreasing trend, with vegetation resistance gradually increasing. CO<sub>2</sub> fertilization enhances vegetation drought resistance, but the magnitude of resistance increase is reduced due to the adverse effects of water stress and VPD on vegetation. The findings of this study may advance our comprehension of terrestrial ecosystem vulnerability and response to drought, and further provide scientific guidance for watershed water allocation, drought preparedness and risk management.

**Keywords:** Drought; SPEI; GPP; Trigger threshold; Threshold dynamics

## 1. Introduction

Terrestrial gross primary productivity (GPP) is the largest flux in the global carbon budget, which is the total amount of organic carbon fixed by vegetation through photosynthesis, and plays an irreplaceable role in offsetting anthropogenic CO<sub>2</sub> emissions and mitigating global warming (Alsafadi et al., 2022; Wang et al., 2021; Xiao et al., 2019; Xu et al., 2019a). As a key element in regulating the carbon cycle, GPP is highly sensitive to climate variability. Therefore, GPP has become an important indicator for studying the relationship between global climate change and terrestrial ecosystems.

To some extent, drought intensity and duration determine the impact of drought on vegetation productivity (Mahecha et al., 2022; Ruppert et al., 2015; Zeiter et al., 2016). In general, drought limits the ability of vegetation to sequester carbon in two ways (Lai et al., 2018; Zscheischler et al., 2014a): the physiological response of plants to drought and the structural changes of vegetation during drought. On the one hand, the physiological responses of vegetation to drought include a reduction in photosynthetic enzymes activity and closure of stomata to prevent water loss, thereby reducing GPP by affecting photorespiration and water availability (Buttler et al., 2018). On the other hand, drought-induced changes in vegetation function and structure may also lead to a reduction in GPP, including reduced stem and leaf growth in trees as drying minimizes water loss through cuticular tissue (Choat et al., 2018; Liu et al., 2017). Even worse, several studies demonstrated that the consequences of vegetation mortality due to drought may adversely affect carbon sinks in terrestrial ecosystems (Delbart et al., 2010; Mcdowell et al., 2010), with potential negative impacts on

terrestrial carbon sequestration (Huang et al., 2016; Xu et al., 2019a).

Based on the above two aspects, drought affects ecosystem productivity by limiting vegetation growth stages, which may ultimately affect the global CO<sub>2</sub> balance (Jiao et al., 2021; Yu et al., 2017). Meanwhile, a large number of studies have found that the effects of drought on ecosystem primary productivity are becoming more frequent globally (Buttler et al., 2018; Deng et al., 2021; He et al., 2020). Researchers have studied the effects of drought on carbon dynamics in different regions, and the results show that drought is offsetting the increase in GPP caused by global warming. For example, a severe drought and heat wave in Europe in 2003 reduced GPP by 30% and led to a significant release of carbon into the atmosphere, reversing four years of net ecosystem carbon sequestration and affecting a wide range of local land cover types (Ciais et al., 2005). Satellite-derived vegetation indices show that ecosystem productivity in semi-arid areas of southeastern Australia is more sensitive to drought than arid and wet ecosystems (Ma et al., 2015). Typically, drought occurs simultaneously with high temperature, and the interaction of the two leads to a significant decrease in GPP (He et al., 2021). The droughts and heat waves that occurred in 1989 and 2008 in the Northeast and Middle East disrupted the carbon cycle (Alsafadi et al., 2022). Researchers used 10 ecosystem models to examine the effects of drought on the carbon cycle in global terrestrial ecosystems. The results showed that drought reduced GPP to a large extent and total respiration (TR) to a lesser extent (Zscheischler et al., 2014b). It is clear that the carbon sequestration capacity of terrestrial ecosystems may be strongly affected by drought in a relatively short period of time, and that severe drought stress has already caused an extremely negative impact on terrestrial ecosystem productivity in several regions around

the world. Therefore, studying the response of vegetation to drought is critical to better understand the relationship between ecosystem carbon cycle and climate change.

China has a diverse range of climatic vegetation types and rich biomes, and its terrestrial ecosystems contribute significantly to the global terrestrial carbon sink. In the past, severe drought events have occurred frequently, causing severe damage to terrestrial ecosystems, economy and society, and food security in China (Gu and Liu, 2015; Li et al., 2022a; Qu et al., 2018; Yan et al., 2021; Yang et al., 2018; Zhang et al., 2020). In 2010, southwest China experienced a severe and persistent spring drought that affected 74% of the total study area and reduced total GPP by about 4% (65 Tg C yr<sup>-1</sup>), resulting in the lowest GPP in the 2000-2010 period (Li et al., 2019b; Zhang et al., 2012; Zhang and Yamaguchi, 2014). In 2013, southern China suffered a once-in-a-century heat wave and summer drought, resulting in a significant reduced GPP and the largest negative crop yield anomaly since 1960 (Yuan et al., 2016). In northeast China, mild drought with higher temperature may increase vegetation productivity, while weak intensity drought exacerbates the lagged effect of ecosystem response to drought (Sun et al., 2016). Apparently, drought has become one of the most important disturbances to vegetation growth in China. Overall, these studies can provide very useful information on the response and vulnerability of terrestrial ecosystems to drought (Chen et al., 2019b).

Despite our growing understanding of the underlying mechanisms of drought-vegetation effects, predicting the extent to which drought severity affects GPP remains difficult. Sun et al. (2016) found that the occurrence of drought does not always result in vegetation loss. Due to vegetation physiological characteristics, soil water buffering and CO<sub>2</sub> fertilization, there are

lagging and accumulation effects of drought on vegetation growth (Fang et al., 2019; Liu et al., 2014; Wei et al., 2022), and vegetation loss is triggered only when drought reaches a certain degree of severity. Therefore, we define the drought trigger thresholds for vegetation as the severity of drought corresponding to different levels of vegetation loss. Assessing the extent to which a meteorological drought triggers a loss of vegetation productivity helps to identify the critical drought state corresponding to the triggering vegetation loss. Current drought thresholds studies have mainly focused on the propagation thresholds from precipitation or meteorological drought to hydrological drought (Guo et al., 2020; Li et al., 2022b; Yue et al., 2022). For example, Guo et al. (2020) studied the meteorological drought propagation thresholds corresponding to different levels of hydrological drought based on copula's conditional probability model. To investigate the drought propagation thresholds that trigger different hydrological drought scenarios, Yue et al. (2022) developed an improved drought propagation model including cumulative precipitation deficit, drought duration, and drought severity. The likelihood of regional vegetation drought and the ability of vegetation to recover from disturbances induced by drought conditions have also been investigated under changes in temperature, precipitation, and soil water content (Fang et al., 2019; Jha et al., 2019). Overall, previous studies have shed some light on the propagation mechanisms between meteorological drought and vegetation loss, providing valuable insights into drought impacts studies. However, previous studies ignored the strength of threshold at which meteorological drought triggers vegetation loss, and few studies assessed the thresholds from meteorological drought to vegetation loss in a probabilistic manner. The resolution of trigger thresholds can also help predict the impact of drought on vegetation health or food security.

Therefore, we need to explore whether there are regional differences in trigger thresholds. Do thresholds exist for all vegetation? Furthermore, the state of vegetation loss due to meteorological drought should theoretically vary in the context of global warming, but the dynamic response mechanisms of vegetation to drought have not been revealed in previous studies. Since the dynamics of trigger thresholds can well reflect the weakening or strengthening of vegetation resistance to drought, and provide scientific guidance for establishing drought early warning models, ignoring the dynamic evolution will reduce the robustness of the study results, and affect the prediction of future vegetation response to extreme climate events such as drought. More importantly, how different factors affect the spatial patterns of trigger threshold dynamics is also an issue that needs to be urgently explored. Further research on the driving factors of trigger threshold dynamics can help decision makers to come up with reasonable and reliable prognosis for drought resilience measures to maintain vegetation health and a sustainable carbon cycle.

Therefore, there is a need to explore the dynamics and drivers of drought trigger thresholds in changing environments to better manage water resources and reduce the impact of drought. The specific objective of this study is to identify the response time of vegetation to drought through correlation analysis. Based on the drought trigger thresholds framework of copula function and conditional probability, the drought trigger threshold for different vegetation losses in the growing season (5-9 month) was calculated (Xu et al., 2019b). Finally, the dynamics of the trigger thresholds were analyzed using a moving window to explore their relationship with hydrometeorological factors.

## **2. Study area and data**

## 2.1. Study area

China is located in the eastern part of the Eurasian continent and on the west coast of the Pacific Ocean. The terrain is high in the west and low in the east, with a terraced topographic distribution. The eastern part of China has obvious monsoon climate characteristics, while the inland northwest has obvious continental climate characteristics. In addition, the spatial and temporal distribution of precipitation is uneven, mostly concentrated in the summer and autumn seasons, while precipitation decreases from the southeast coast to the northwest inland. Based on the vegetation types and their geographic distribution, eight vegetation-climate zones (Fig.1) have been identified, including cold temperate coniferous forest region(R1), temperate coniferous and broad-leaved forest region (R2), warm temperate deciduous broad-leaved forest region (R3), subtropical evergreen broad-leaved forest region (R4), tropical monsoon rain forest and rain forest region (R5), temperate grassland region (R6), temperate desert region (R7) and alpine vegetation region of Qinghai-Tibet plateau (R8).

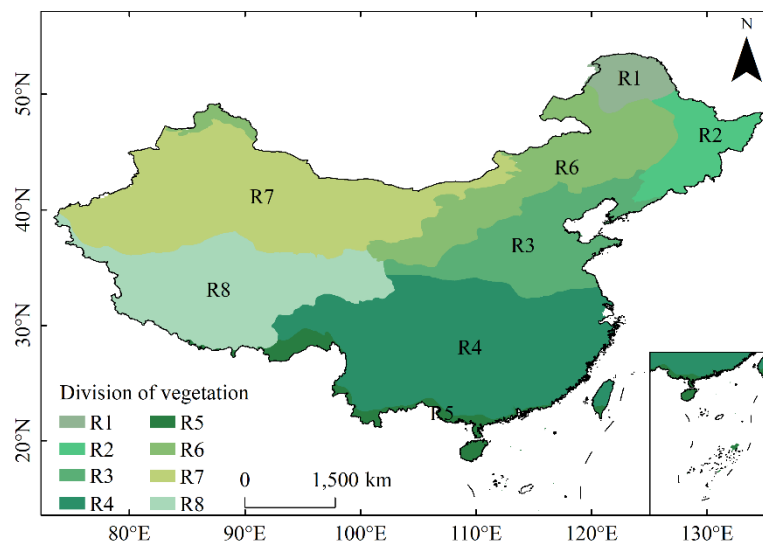


Fig.1 Vegetation division in China (cold temperate coniferous forest region(R1), temperate coniferous and broad-leaved forest region (R2), warm temperate deciduous broad-leaved forest region (R3), subtropical

evergreen broad-leaved forest region (R4), tropical monsoon rain forest and rain forest region (R5), temperate grassland region (R6), temperate desert region (R7), alpine vegetation region of Qinghai-Tibet plateau (R8)).

## 2.2. Data

The Chinese vegetation zone data from the Resource and Environment Science and Data Center is used in the study. The map reflects in detail the regional distribution and zonal differentiation of vegetation in 36 sub-regions of the 8 major vegetation regions in China (<https://www.resdc.cn/>). The global GPP dataset with a spatial resolution of  $0.05^\circ$  and 8 days interval used in this study was generated by using the revised eddy covariance light use efficiency model (EC-LUE model) which can better simulate the spatial, seasonal and interannual changes of global GPP (<https://doi.org/10.6084/m9.figshare.8942336.v3>). GPP-GLASS and GPP-Sun products are obtained from the National Earth System Science Data Center, National Science & Technology Infrastructure of China (<http://www.geodata.cn>). The monthly SPEI (SPEI base v2.6) dataset from 1982 to 2018 with time scales ranging from 1 to 12 months at a spatial resolution of  $0.5^\circ$  is obtained from the CSIC (<http://digital.csic.es/handle/10261/202305>). The atmospheric  $\text{CO}_2$  observations at Mauna Loa Observatory is obtained from the NOAA Earth System Research Laboratories (<https://gml.noaa.gov/ccgg/trends/data.html>). Monthly air temperature (TMP) and vapor pressure datasets with  $0.5^\circ$  spatial resolution are obtained from the Climate Research Unit (CRU) at the University of East Anglia (CRU TS v4.05). They are used to calculate the atmospheric water vapor pressure deficit (VPD). The root zone soil moisture (SM) products used in this study come from the GLDAS with a spatial resolution of  $0.25^\circ \times 0.25^\circ$ , and

ERA5 SM data is acquired from <https://cds.climate.copernicus.eu/cdsapp#!/search>. The Fraction of Absorbed Photosynthetically Active Radiation (FAPAR) dataset is obtained from the University of Maryland GLASS Products, which were generated from multi-source remote sensing data and ground measured data (<http://glass-product.bnu.edu.cn/>). Note that GPP, SM and FAPAR were resampled to  $0.5^\circ \times 0.5^\circ$  using the mean aggregation method.

### **3. Methods**

#### *3.1. Standardized Precipitation Evapotranspiration Index*

The Standardized precipitation evapotranspiration index (SPEI) can describe the drought status of a region by the deviation of the difference between precipitation and potential evapotranspiration from the mean state. The cumulative series of water losses and gains at different time scales ( $D = P - ET_0$ ) is first obtained from the monthly P and  $ET_0$  data. Then the cumulative probability density is normalized using the three-parameter logistic probability distribution function to obtain the SPEI for multiple time scales (Vicente-Serrano et al., 2010). The monthly potential evapotranspiration ( $ET_0$ ) required for calculating SPEI was estimated using the FAO-56 Penman-Monteith (PM) formula. Compared with the temperature-based Thornthwaite equation, the  $ET_0$  estimated by FAO-56 PM is superior to that calculated by Thornthwaite (Feng et al., 2017), as it integrates aerodynamic and energy balance theories and takes into account the effects of temperature, solar radiation, wind speed and relative humidity on  $ET_0$ . Subsequently, it is recommended by FAO as the standard formula for calculating  $ET_0$  in 1998. Drought indices at multiple time scales are critical for assessing the response time of vegetation status to drought conditions. In this study, the response time is defined as the time scale that has the greatest SPEI-GPP correlation (Fang et al., 2019; Han et al., 2021;

Vicente-Serrano et al., 2013).

### 3.2. Copula-based drought trigger threshold for vegetation productivity loss

Satellite-observed vegetation trends are the result of the combined responses of vegetation to climate change, rising atmospheric CO<sub>2</sub> concentrations, nitrogen deposition, and land-use change (Chen et al., 2019a; Piao et al., 2019; Tagesson et al., 2020). To investigate the impact of different levels of drought on vegetation productivity loss while minimizing the effects of other confounding factors on trigger thresholds (Yang et al., 2016), we performed linear detrending of GPP for each pixel and calculated trigger thresholds using the following framework (Liu et al., 2018; Zscheischler and Seneviratne, 2017).

#### 3.2.1. Joint distribution

Copula function is a multivariate joint distribution function proposed by Sklar in 1959 (Sklar, 1959), which has the advantage of being flexible enough to connect two or more random variables with different marginal distributions. In this study, the two-dimensional copula function was used to construct the joint distribution of SPEI and GPP series (see Eq. (1)).

$$F_{SPEI-i,GPP}(SPEI, GPP) = C(F_{SPEI-i}(SPEI), F_{GPP}(GPP)) \quad (1)$$

where  $SPEI-i$  is the SPEI scale corresponding to the response time of each pixel.  $F_{SPEI-i,GPP}$  is the joint distribution,  $F_{SPEI-i}$  and  $F_{GPP}$  are marginal distributions of the  $SPEI_i$  and GPP series, respectively.  $C()$  denotes a copula function, and Clayton, Frank, Gumbel, Gaussian and t Copula are selected as alternative joint distribution functions in this study. Two types of candidate distributions (i.e., normal distribution, generalized extreme value distribution) were fitted to the GPP series. The best marginal distribution was selected based on the

Kolmogorov-Smirnov test (K-S test) and the root mean square error (RMSE). The normal distribution was used to fit the SPEI since it was the exponent with the standard normal transformation. The Copula function was then tested for goodness of fit using the squared Euclidean distance (SED), and the distribution with the least squared Euclidean distance was considered to be the optimal joint distribution.

### *3.2.2. Conditional probability*

In this study, the copula-based joint and conditional distribution equations (see Eq. (2)) were used to calculate the probability of vegetation loss under different drought stresses i.e. mild drought ( $-1 < \text{SPEI} \leq -0.5$ ), moderate drought ( $-1.5 < \text{SPEI} \leq -1$ ), severe drought ( $-2 < \text{SPEI} \leq -1.5$ ) and extreme drought ( $\text{SPEI} \leq -2$ ). Regarding the determination of vegetation loss, some studies have used NPP's Z-score to explore global carbon sink anomalies (Poulter et al., 2014), and the Z-score method improves data comparability by making the data dimensionless. However, the Z-score weakens data interpretation, while the percentile method, a non-parametric method applicable to data from a variety distribution types, is highly operable to characterize vegetation loss. For example, Konings et al. (2017) used NDVI deficit percentile to explore the sensitivity of its variation to VPD, and the percentile method has also been used to characterize the extremes of vegetation carbon sequestration capacity and to monitor real-time crop growth (Korth et al., 2015; Li et al., 2019a). Therefore, the percentile method was used to determine the vegetation productivity loss scenarios, and four types of vegetation losses are defined as GPP less than or equal to  $\text{GPP}^{40\text{th}}$ ,  $\text{GPP}^{30\text{th}}$ ,  $\text{GPP}^{20\text{th}}$  and  $\text{GPP}^{10\text{th}}$ , and then the probability of vegetation loss under each level of drought stress was calculated separately.

Probability of vegetation loss under drought stress is calculated as:

$$\begin{aligned}
 P(GPP \leq gpp | u_1 < SPEI \leq u_2) &= \frac{P(u_1 < SPEI \leq u_2, GPP \leq gpp)}{P(u_1 < SPEI \leq u_2)} \\
 &= \frac{F_{SPEI,GPP}(u_2, gpp) - F_{SPEI,GPP}(u_1, gpp)}{F_{SPEI}(u_2) - F_{SPEI}(u_1)}
 \end{aligned} \tag{2}$$

where  $u_1$  and  $u_2$  are the upper and lower limits of the given interval of SPEI.

### 3.2.3. Determination of trigger thresholds

In section 3.2.2, we specify the possibility of certain loss of vegetation when a certain drought occurs. In addition, the extent to which vegetation can withstand drought is also an important part in the research of vegetation response to climate. Therefore, the study focuses on the SPEI threshold for a certain level of vegetation loss. According to the classification criteria of the drought index, a SPEI index below -2 is considered to be an extreme drought. We understand that the minimum SPEI value will not be lower than -3 in most areas of China, so we use -3 as the lower limit of the threshold interval (Yao et al., 2020). As shown in Fig.2, the response time of each grid was determined first, and then the joint distribution of GPP and SPEI of the maximum time scale was constructed grid by grid. Finally, vegetation loss for  $GPP \leq GPP^{40th}$  is set, and SPEI is iterated from -0.5 at an interval of 0.1. By combining the vegetation loss probability assessment model with the trial algorithm, the conditional probability corresponding to each iteration can be estimated (see Eq. (3)). When the conditional probability is greater than or equal to 0.5, the corresponding SPEI interval is returned, and the left side of the interval is considered as the trigger threshold, which is the SPEI corresponding to the induced vegetation loss. When the trigger threshold is low (the smaller SPEI), it means that the occurrence of a higher level of meteorological drought will cause the specified vegetation loss, indicating that the vegetation is more resistant to

meteorological drought. Conversely, when the trigger threshold value is higher (the larger SPEI), it indicates that the occurrence of a lower level of meteorological drought will trigger vegetation loss. In addition, to enhance the robustness of the conclusions, we used multiple GPP datasets to analyze the thresholds and their dynamics.

$$P(GPP \leq gpp | x_{i-0.1} < SPEI \leq x_i) = \frac{F_{SPEI,GPP}(x_i, gpp) - F_{SPEI,GPP}(x_{i-0.1}, gpp)}{F_{SPEI}(x_i) - F_{SPEI}(x_{i-0.1})} \quad (3)$$

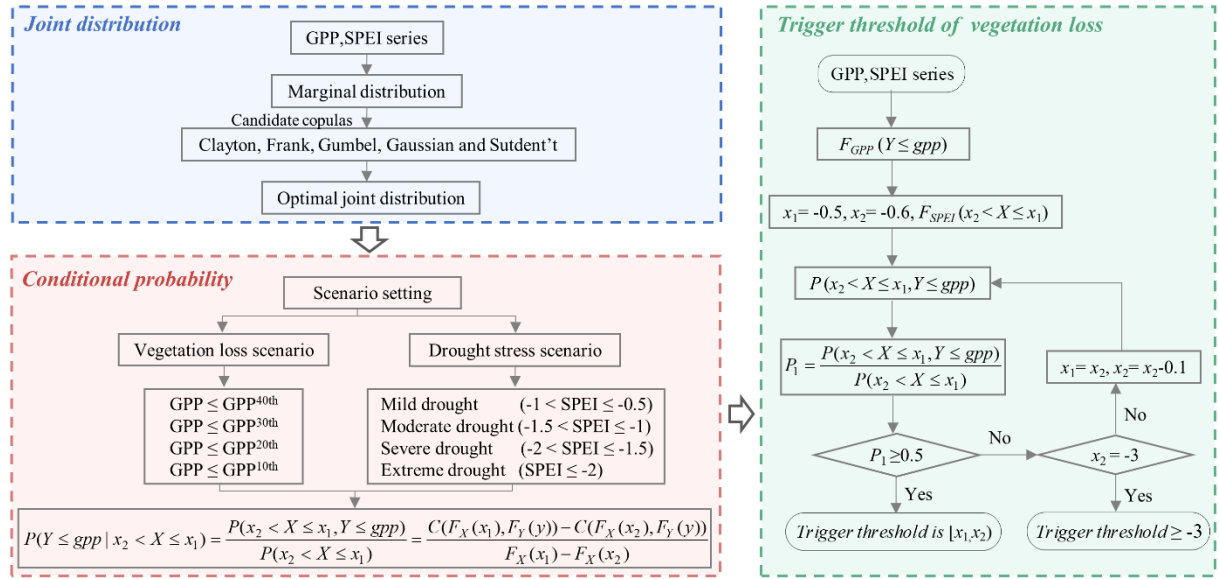


Fig.2 Framework for determining drought trigger thresholds of various vegetation losses.

### 3.3 Random forest regression model

Random Forest (RF) model is a classification tree based machine learning algorithm proposed by Breiman in 2001 (Breiman, 2001). The model uses resampling method to extract multiple samples from the original sample, builds decision tree modeling for each sample, and then combines multiple decision trees for prediction. RF is insensitive to multivariate covariance, and the results are more robust to missing data and unbalanced data, and the effects of up to several thousand explanatory variables can be well predicted (Zhang et al., 2014; Zhu et al., 2015). Due to its distinct and unique algorithm advantages, RF is able to assess the importance of each parameter on the response, so we used random forest importance scores to identify important variables. Based on the above, the RF algorithm was adopted to construct a correlation model between trigger thresholds and climate variables to

assess the influence of variables on the dynamics of trigger thresholds.

## 4. Results

### 4.1. Response time of GPP to meteorological drought

To determine the response time of vegetation productivity to moisture changes in China, the growing season GPP series were correlated with SPEI over multiple time scales (1-12 months). As illustrated in Fig. 3a, the correlation of GPP-SPEI indicates a clear spatial heterogeneity, with vegetation productivity and SPEI being strongly positively correlated, particularly in the northern part of R4, where the correlation coefficient may exceed 0.6. This indicates that the variations in vegetation productivity (i.e., carbon sequestration) are consistent with the variations in SPEI in these areas. The GPP-SPEI is positively correlated for most parts of R7. R7 is a temperate desert region, located in an arid region with sparse vegetation and scarce water (Fig. 3b). R8 is located on the Qinghai-Tibet Plateau, and GPP-SPEI is negatively correlated in its eastern region. It has been proven that GPP changes are affected not only by water availability, but also by human activities and soil moisture content in the eastern R8, where the intensity of human activities and soil moisture content are higher than those in the western Qinghai-Tibet Plateau (Fan et al., 2019; Jiang et al., 2020). In addition, it has also been shown that temperature has a greater effect on productivity than precipitation, and in summary, more wet conditions may not stimulate the GPP (Ma et al., 2018; Yuan et al., 2021). Due to the combined effects of multiple factors, the ecological vulnerability of vegetation to meteorological changes is higher in the east than in the west (Zhang et al., 2022b).

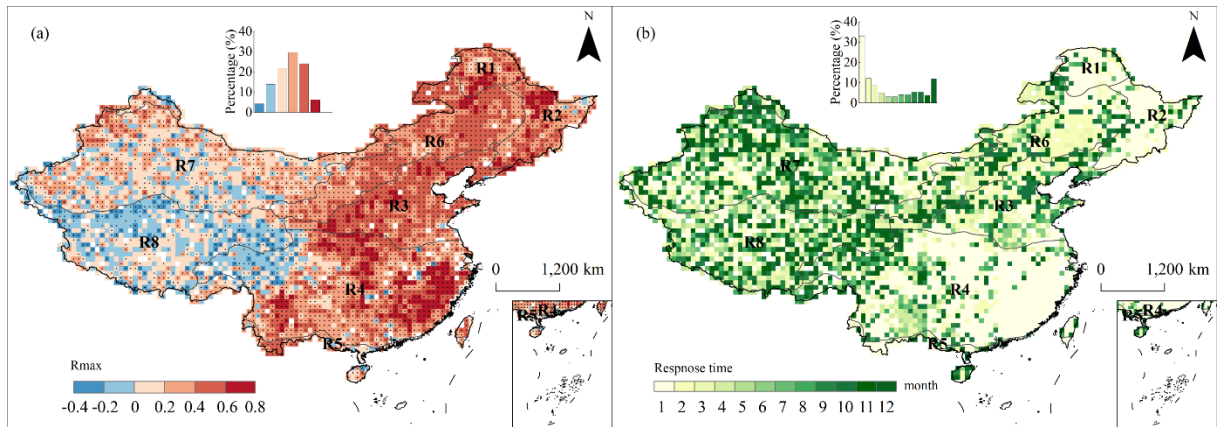


Fig.3 Maximum correlation coefficient and response time between GPP and SPEI in growing season (a) spatial distribution of maximum correlation coefficient, (b) spatial distribution of response time corresponding to maximum correlation coefficient. The black dots indicates significant correlation ( $P < 0.05$ ).

The study used the time scale corresponding to GPP-SPEI maximum correlation to analyze the spatial distribution of the response time of vegetation productivity to water availability. According to the correlation analysis, the response time of 59.79% of terrestrial ecosystems to water resources in China is mainly based on short-term (less than 4 months) time scales (Fig.3b). Response times are relatively short in southern and northeastern China (R1 and R2). In contrast, the response time is typically more than 9 months (accounting for 26.62% of the total area of China) in northeastern China (parts of R3 and R6) and arid and semi-arid regions. Especially in the northwest arid region, the longer response time (more than 12 months) of vegetation to drought may be related to the adaptation of vegetation to water deficit in semi-arid ecosystems, where vegetation develops resistance to drought and is more adapted to longer response time (Huang et al., 2016). For example, vegetation resists drought disturbance by transporting water through the deep root system and regulates hydraulic redistribution to promote its growth (Saleska S R et al., 2007). The longer the

response time to changes in water availability, the greater the capacity of vegetation productivity in these areas to withstand chronic water scarcity, whereas the shorter the response time, the lower the capacity to withstand water scarcity. A similar study also found that the impact of drought on net ecosystem production capacity (NEP) had a short-term lag (1-3 months) in the humid and warm regions of eastern China, while the impact of drought on NEP is relatively weak but lasts for a long time in the cold and arid western regions (Liu et al., 2014).

#### *4.2. Probability of triggering vegetation productivity loss under different drought scenarios*

The copula function was used to systematically assess the probability of vegetation productivity loss. This section examines the conditional probability of occurrence of different levels of vegetation productivity loss (below the 40th, 30th, 20th, and 10th percentile of GPP) under four meteorological drought scenarios (i.e., mild, moderate, severe, and extreme drought), where the lower percentile value, the more severe the damage to ecosystem health from drought. Our results demonstrate that the proportion of high probability and area of triggering vegetation productivity loss is expected to increase with the intensity of drought (Fig.4), indicating higher vegetation vulnerability owing to severe water deficit during the growing season. When  $GPP \leq GPP^{40th}$ , the area fraction of probability higher than 80% is only 2.04% under moderate drought, while this proportion increases to 4.87% under severe drought and up to 27.78% under extreme drought conditions. Moreover, when GPP is subjected to different loss situations, it still shows the same variation characteristics.

Similarly, the probability and area of triggering severe vegetation loss decrease gradually as the GPP loss level increases for the same level of drought stress. Under the drought

scenarios, northeastern and southeastern China are significantly more likely to experience vegetation productivity loss risk than the northern China. Specifically, southern and northeastern China are areas with a high probability of compound dry heat events, making vegetation productivity more vulnerable in these two regions (Li et al., 2021; Li et al., 2019c; Wu and Jiang, 2022). Overall, despite being located in a humid region with abundant rainfall, the southeast is still at risk of drought, with a high probability of vegetation productivity loss, and vulnerability to vegetation health. Therefore, it is crucial to further determine the thresholds that trigger vegetation productivity loss to mitigate the effects of drought on ecosystem health in a timely and effective manner.

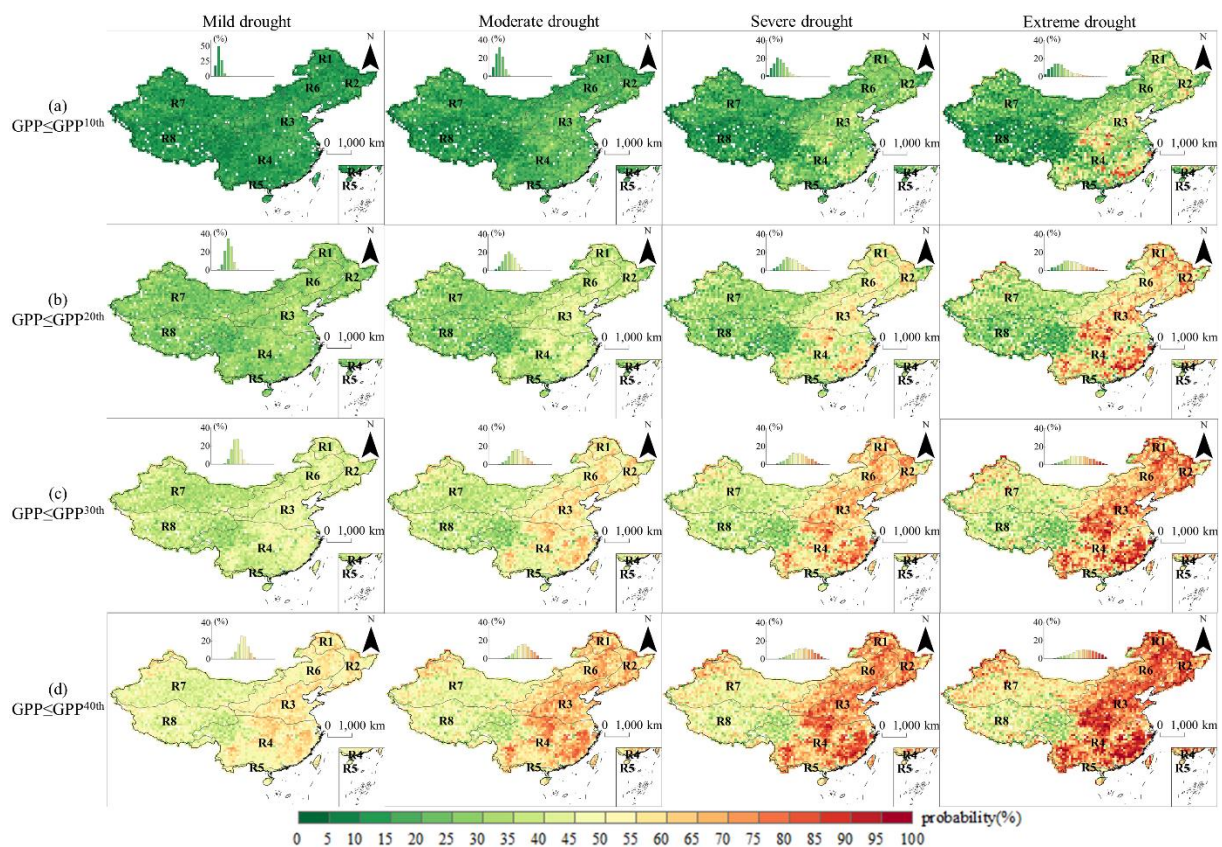


Fig.4 Conditional probabilities of the vegetation productivity loss under different drought scenarios (mild, moderate, severe and extreme drought) in growing season (a)  $GPP \leq GPP^{10th}$ , (b)  $GPP \leq GPP^{20th}$ , (c)  $GPP \leq GPP^{30th}$ , and (d)  $GPP \leq GPP^{40th}$ .

### 4.3. Trigger thresholds from meteorological drought to GPP loss

When the trigger threshold is small (purplish), it indicates that only the occurrence of higher-grade drought can cause vegetation loss, which means that the vegetation has strong resistance to drought (Fig. 5). Conversely, observed reddish regions indicates that lower-grade drought can trigger vegetation loss and vegetation is vulnerable to drought events. Moreover, for  $GPP \leq GPP^{40th}$ , the percentages of pixels with trigger thresholds are 58.11%, 11.28%, 4.97%, and 3.91% for mild, moderate, severe, and extreme drought, respectively. The high trigger threshold area of vegetation productivity loss is located in eastern China. The most vulnerable R4 region may be related to the frequent seasonal droughts and the presence of a significant soil drought trend in the area with high GPP vulnerability (Chen et al., 2021a; Chen et al., 2021b; Green et al., 2019; He et al., 2021). As a result, in the event of mild drought, southeastern China is prone to vegetation loss with  $GPP \leq GPP^{40th}$ , with similar conclusions confirmed by  $GPP \leq GPP^{30th}$ ,  $GPP \leq GPP^{20th}$ , and  $GPP \leq GPP^{10th}$ .

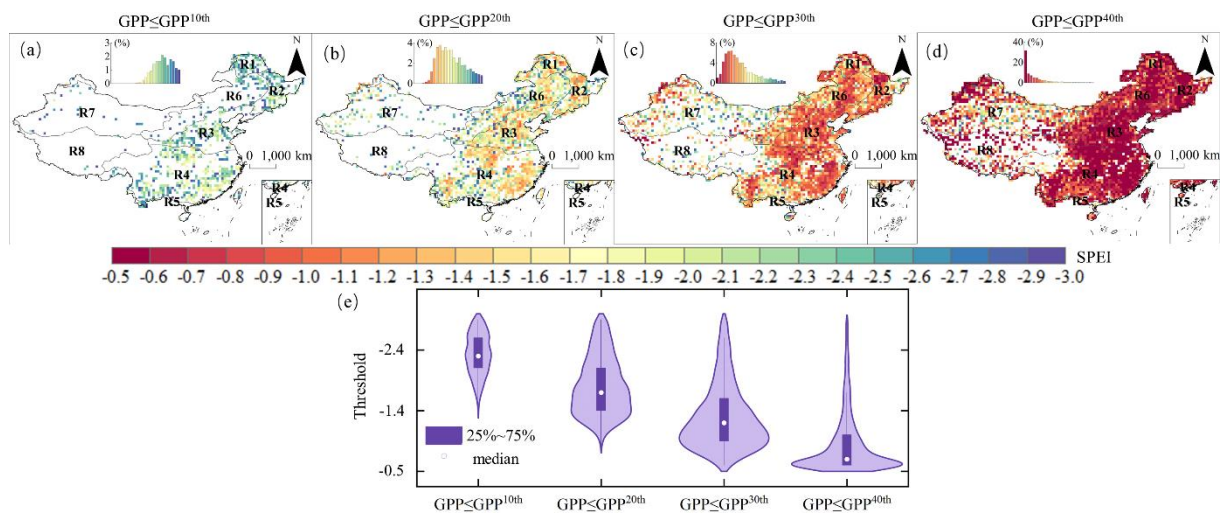


Fig.5 Trigger thresholds for vegetation productivity loss. Spatial distribution of trigger threshold for (a)  $GPP \leq GPP^{10th}$ , (b)  $GPP \leq GPP^{20th}$ , (c)  $GPP \leq GPP^{30th}$ , (d)  $GPP \leq GPP^{40th}$ , and (e) the violin plot reflecting the distribution and probability density of trigger thresholds. The upper and lower limits of the trigger

threshold are -0.5 and -3, respectively.

The preliminary analysis of trigger thresholds can be shown in Fig.5e. It can be seen that the PDF curve shifts upward with increasing vegetation productivity loss, implying that the drought threshold for triggering vegetation loss is decreasing, suggesting that more severe drought is required to trigger greater vegetation loss and the risk of GPP reduction is reduced.

#### *4.4 Dynamic evolution of trigger thresholds*

##### *4.4.1 Spatial distribution of dynamic evolution of trigger thresholds*

To evaluate the long-term trend of trigger thresholds changes, we used a 15-year moving window to test the dynamic changes of trigger thresholds. Based on the 15-year moving window, the above framework was used to calculate the trigger threshold for  $GPP \leq GPP^{40th}$  under each window. In northeastern China (R1, R2, and R6), the trigger thresholds show a decreasing trend, which indicates that the resistance of vegetation gradually increases with time change (Fig. 6a). In contrast, vegetation has reduced resistance in part of R3 and is vulnerable to lower levels of drought. The Huang-Huai-Hai Plain in the R3 region is one of the major crop-producing areas in China. Due to the long-term over-exploitation of groundwater for irrigation and urban water use, the groundwater leakage is expanding and water shortage is prominent (Su et al., 2020; Sun et al., 2020). In addition, the vegetation productivity in the region is vulnerable to drought and therefore has reduced drought resistance (Shi et al., 2020). As seen in Fig 6b, the vegetation resistance shows an increasing trend in terms of temporal changes.

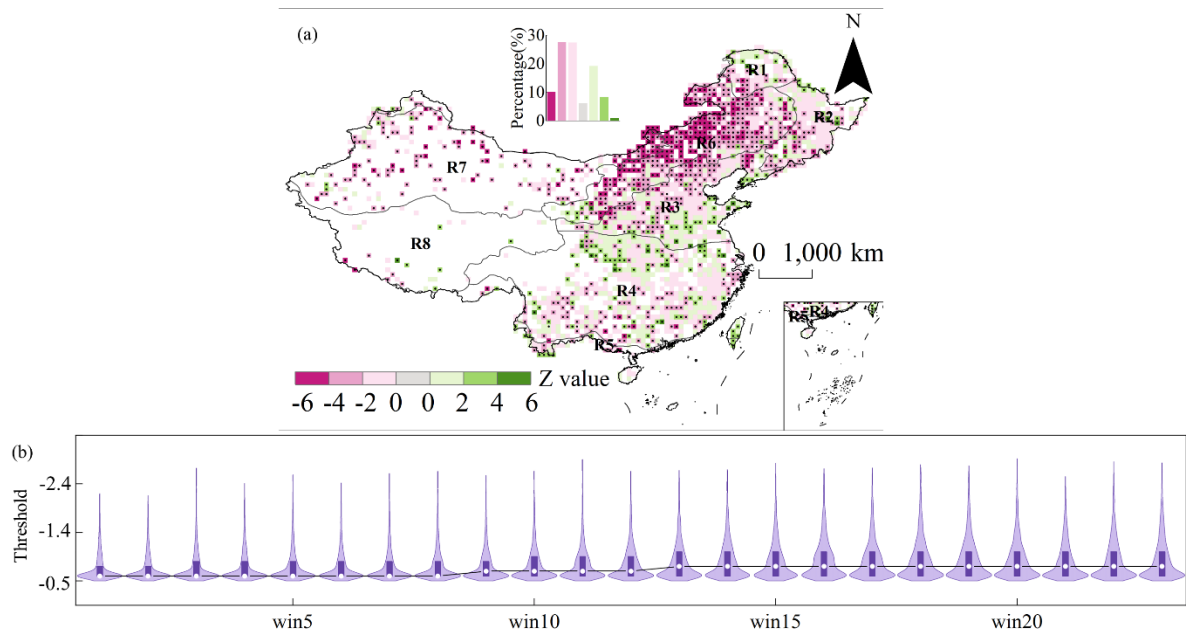


Fig. 6 Dynamics of the trigger threshold for  $GPP \leq GPP^{40th}$  (a) MK test Z values for thresholds, and (b) distribution of trigger thresholds. The black line is the connecting line for the median trigger threshold of each window.

#### 4.4.2 Driving factors affecting the variation of trigger thresholds

To investigate the causes of changes in trigger thresholds, random forest variable importance scores were calculated to assess the effects of  $CO_2$ , TMP, VPD, SM, and FAPAR on the trigger thresholds (Breiman, 2001; Zhang et al., 2014; Zhu et al., 2015) (Fig. 7a-e). From Fig. 7f, it can be seen that the goodness of fit of the model can reach above 0.75, and the largest score is identified as the dominant factor for threshold change (Fig. 8) The analysis shows that the dynamics of the trigger threshold is mainly attributed to SM change (Fig. 8a), involving more than 40% of the study region, involving more than 40% of the study region, followed by FAPAR (17.27%), VPD (16.57%), TMP (15.39%), and  $CO_2$  (10.56%), respectively. Previous studies have noted the significance of SM for global long-term terrestrial carbon uptake (Green et al., 2019). Soil moisture, a directly available source of

water for plant photosynthesis (Gao et al., 2021), can constraint total primary production through ecosystem water stress when drought occurs. If soil moisture deficit is high enough to bring soil moisture below the wilting point, it can lead to reduced vegetation function or even death (Anderegg et al., 2015; Madakumbura et al., 2020; Reichstein et al., 2002; Zhao and Running, 2010; Zheng et al., 2022). In addition to SM, VPD also plays a non-negligible role in trigger threshold dynamic (Fig. 8b). Plants respond to high VPD by reducing stomatal conductance to minimize water loss and result in lower light use efficiency, which affects the response of GPP to drought (Grossiord et al., 2020; Wu et al., 2013). In addition, it is also found that the dynamics of trigger threshold can be attributed to the TMP at high altitudes. Jiang et al. (2021) also found that temperature was the main factor affecting GPP variation in the Han River basin (western of R3).

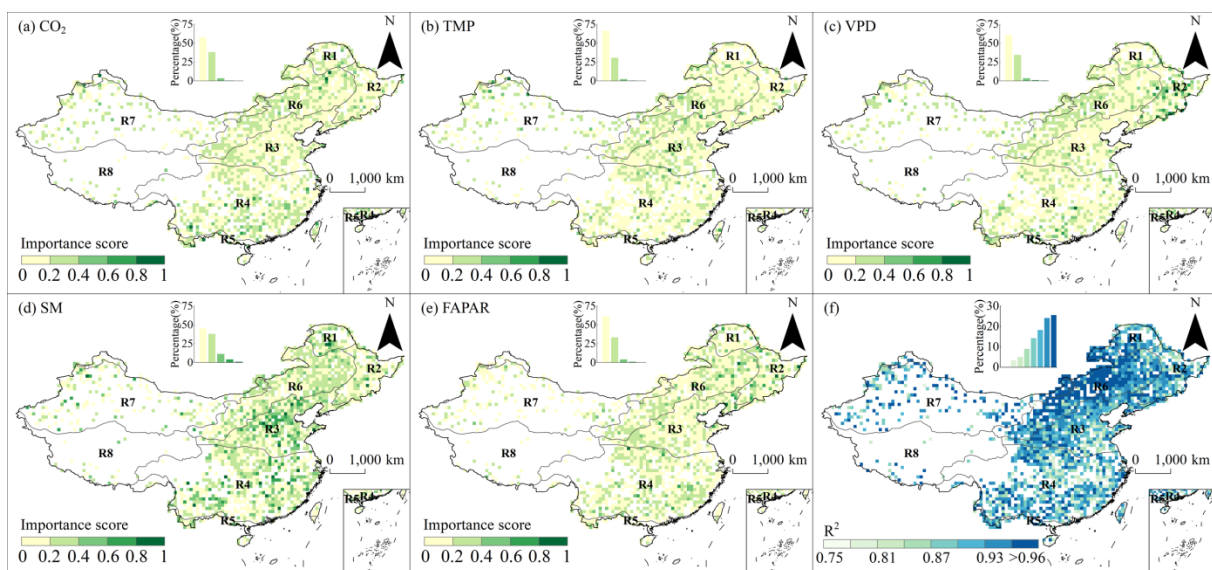
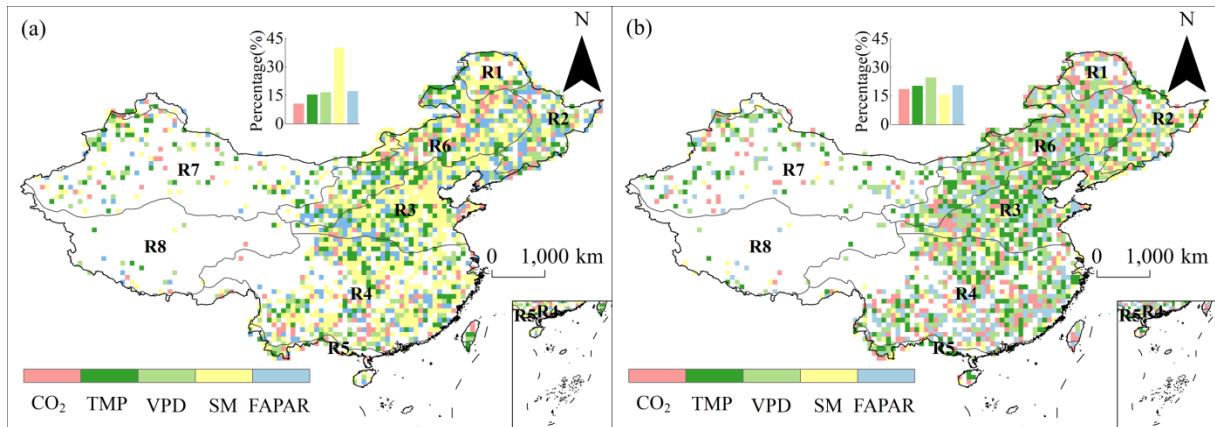


Fig. 7 Importance scores of factors based on random forest (a-e) and the goodness of fit of the model (f).

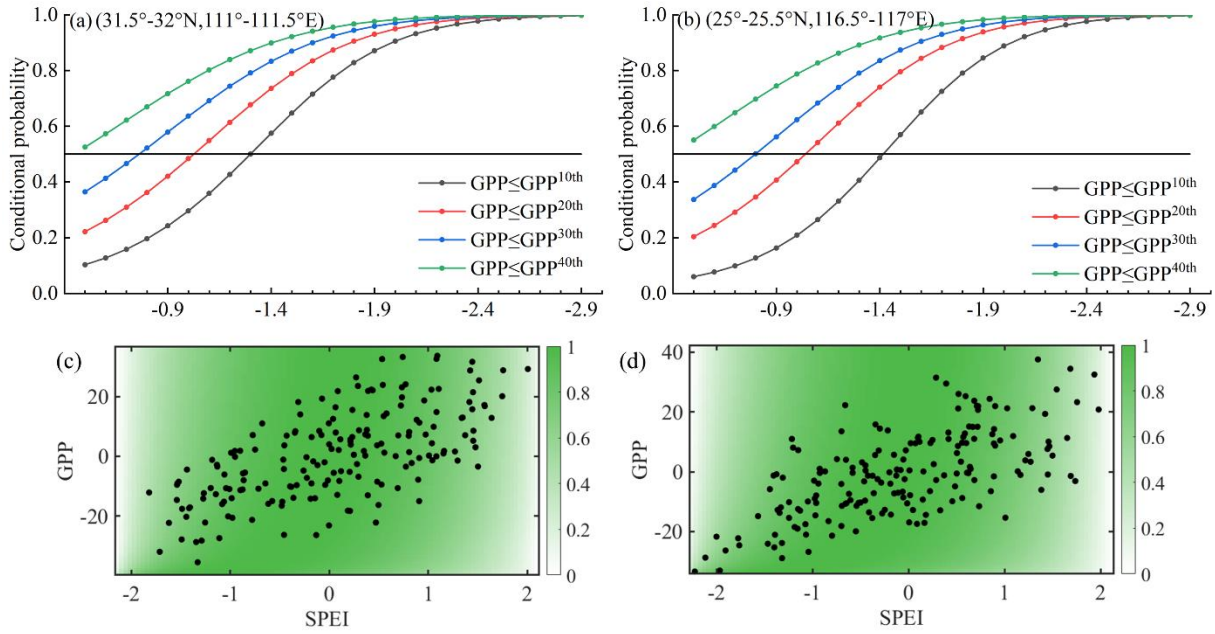


1  
 2 Fig. 8 Driving factors based on random forest importance (a) the most important factor, and (b) the second  
 3 most important factor.

## 4 **5. Discussions**

### 5 *5.1. Reliability verification of the drought trigger thresholds framework*

6 We randomly selected two pixels to analyze the change in probability of occurrence of  
 7 different levels of vegetation loss under different drought conditions (Fig.9a-b). It can be  
 8 clearly seen that the probability decreases with increasing vegetation loss under the same  
 9 drought conditions, while the probability gradually increases with increasing drought under  
 10 the same vegetation loss. In fact, considering that GPP is influenced to some extent by  
 11 environmental factors such as land use change, nitrogen deposition, and CO<sub>2</sub> fertilization  
 12 effects, the occurrence of drought does not necessarily lead to vegetation productivity loss.  
 13 Conversely, vegetation loss may occur when the climate becomes wetter. Based on this  
 14 uncertainty, the use of a probabilistic framework provides a new perspective on the response  
 15 of vegetation productivity to drought. For the whole of China, a conditional probability of 0.5  
 16 was chosen for uniformity. However, for the Chinese sub-regions or other regions, or for finer  
 17 time scales (seasonal, monthly, decadal), higher conditional probabilities can be selected if the  
 18 correlation between GPP and SPEI is higher.



19

20 Fig.9 Validation of the reliability of the trigger threshold framework (a,b) comparison of actual values of  
 21 paired GPP-SPEI with the estimated GPP distribution for two randomly selected pixels, (c,d) conditional  
 22 probability of occurrence of vegetation productivity loss under different drought levels.

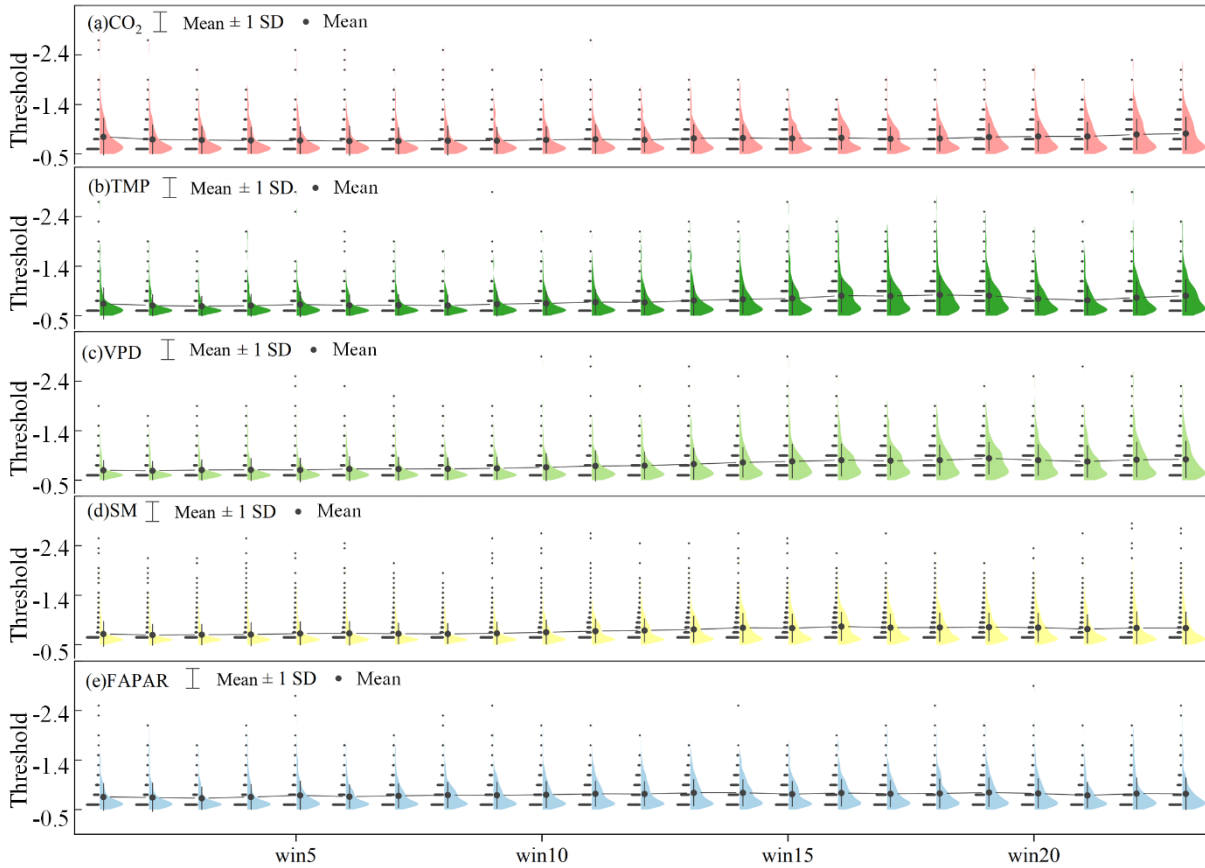
23 On the other hand, the reliability of the trigger threshold framework was verified by  
 24 comparing the estimated GPP conditional density distribution on different SPEI values with  
 25 the paired GPP-SPEI actual values. As illustrated in Fig9.c-d, most of the paired GPP-SPEI  
 26 actual values are located in the high-density areas. Overall, the trigger threshold framework  
 27 established in this study is reliable for studying vegetation productivity losses in response to  
 28 different levels of droughts.

### 29 5.2. Driving factors on the variation of trigger thresholds

30 The pixels corresponding to the dominant factor were extracted and analyzed for changes  
 31 in trigger thresholds under a moving window. As can be seen from Figs. 10, the decreasing  
 32 threshold of the pixels, with  $CO_2$  as the dominant factor, is closely related to  $CO_2$  fertilization,  
 33 and rising  $CO_2$  concentration leads to a concomitant increase in the water use efficiency of

34 vegetation. On the other hand, the physiological effect caused by elevated CO<sub>2</sub> concentration  
35 (stomatal inhibition effect) reduces stomatal conductance and diminishes evaporative losses  
36 and water use by plants, thus increasing water use efficiency and mitigating the trend of  
37 increasing drought frequency (Yang et al., 2019; Zhang et al., 2022a; Zhang et al., 2022c).  
38 Nevertheless, saturation of the fertilization effect may occur if the maximum ecosystem  
39 photosynthesis rate is reached or due to other limiting factors (Joshi et al., 2020). As the  
40 frequency and severity of droughts increase, there is growing evidence that increasing water  
41 stress is the dominant factor driving the response of ecosystem production to drought (Liu et  
42 al., 2020; Zheng et al., 2020; Zhou et al., 2019). The drought resistance of pixels with TMP as  
43 the main factor first increased and then decreased slightly, which may be attributed to the  
44 slowdown of global temperature growth after 1998 (Su et al., 2016), and the positive effect of  
45 climate warming on vegetation growth has weakened (Piao et al., 2017). If the region with  
46 increased evapotranspiration cannot keep up with the growing evapotranspiration demand  
47 (Zhang et al., 2021), it will exacerbate climate drying and cause dryland expansion with  
48 increasing water stress, which will make vegetation more sensitive to drought in later period.  
49 In more severe situations, the combination of very low soil moisture and high VPD  
50 (evapotranspiration demand) can strongly limit carbon uptake and may trigger vegetation  
51 mortality (Gentine et al., 2019; Zhou et al., 2019). In addition, for pixels with SM as the  
52 dominant factor, the positive promotion of CO<sub>2</sub> fertilization effect on vegetation growth is  
53 offset by the negative effect of water deficit, resulting in little change in the effect of SM on  
54 the trigger threshold. Similarly, with the increased proportion of solar radiation absorbed by  
55 photosynthesis, the photosynthetic capacity of vegetation is enhanced, and the ability of

56 vegetation to resist drought is further improved in areas dominated by FAPAR.



57  
58 Fig. 10 The trigger threshold change dominated by CO<sub>2</sub>, TMP, VPD, SM and FAPAR under different  
59 moving windows. (The folded line represents the mean linkage line under the moving window.)

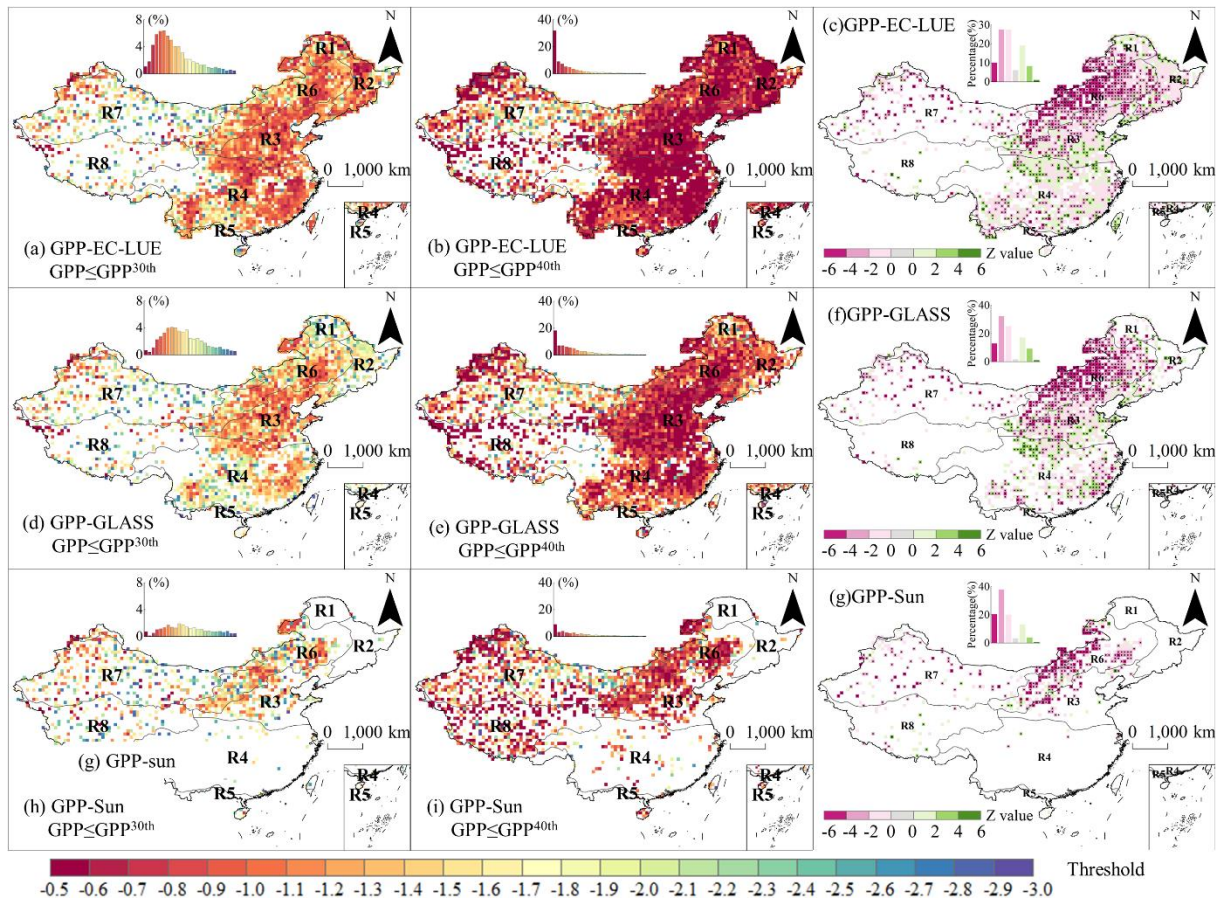
### 60 5.3. Robustness validation of datasets

61 To assess the robustness of the findings, we analyzed the spatial distribution of the  
62 trigger thresholds as well as the dynamics using GPP-EC-LUE, GPP-GLASS and GPP-sun  
63 products (Figs. 11). Among them, GPP-Sun is based on the light utilization model MuSyQ,  
64 which improves the LUE estimation by introducing the Clear Sky Index (CI), and estimates  
65 GPP on this basis. GPP-GLASS has been widely used in global change studies, which adopts  
66 Bayesian integration algorithm and assembles eight light energy utilization models together.  
67 Previous study found that GPP-GLASS may be able to depict the true value of GPP better  
68 than MuSyQ (He et al., 2022). The GPP-EC-LUE used in this study is synthesized by  
69 combining atmospheric CO<sub>2</sub> concentration, radiation composition and VPD through a  
70 modified EC-LUE model. The modified EC-LUE has unique advantages in reproducing the

71 interannual variability of GPP at the site level and global scale.

72         The analysis of the three validation datasets is shown in Fig. 10. It can be seen that there  
73 are similarities in the spatial variation and dynamics of the thresholds of GPP-GLASS and  
74 GPP-EC-LUE, both of which show a gradual increase in vegetation resistance in the northern  
75 region. Although the trend in threshold points is relatively consistent with the first two  
76 datasets, GPP-Sun differs significantly from the first two datasets in the south. The absence of  
77 threshold points in southern China (evergreen broad-leaf forest, R4) may be due to the  
78 influence of factors such as clouds or snow that reduce the reliability of the reflectance used  
79 as input to the algorithm. It is also possible that the MuSyQ algorithm simulates a different  
80 intra-annual distribution of GPP, which would affect the calculation of trigger threshold.  
81 Despite the differences in the GPP datasets, it is clear from the results that all three datasets  
82 show the same variation to some extent at the points where thresholds exist. However, the  
83 points without thresholds in the three datasets may be due to poor coupling between  
84 vegetation and drought, which indicates that the factors driving vegetation loss are lie  
85 elsewhere, such as the in the varying hydrothermal conditions of the basin, groundwater  
86 recharge and water conservancy projects.

87         In addition, we also investigated the importance of threshold dynamic changes using the  
88 SM from ERA5 (Fig. 12). It can be seen that the two SM datasets have similar effects on the  
89 dynamics of the thresholds, albeit with lightly different percentages, with the largest  
90 influencing factor being SM and the second factor being VPD. Combined with the above  
91 analysis, it can be seen that the conclusions drawn from the selected datasets are robust.

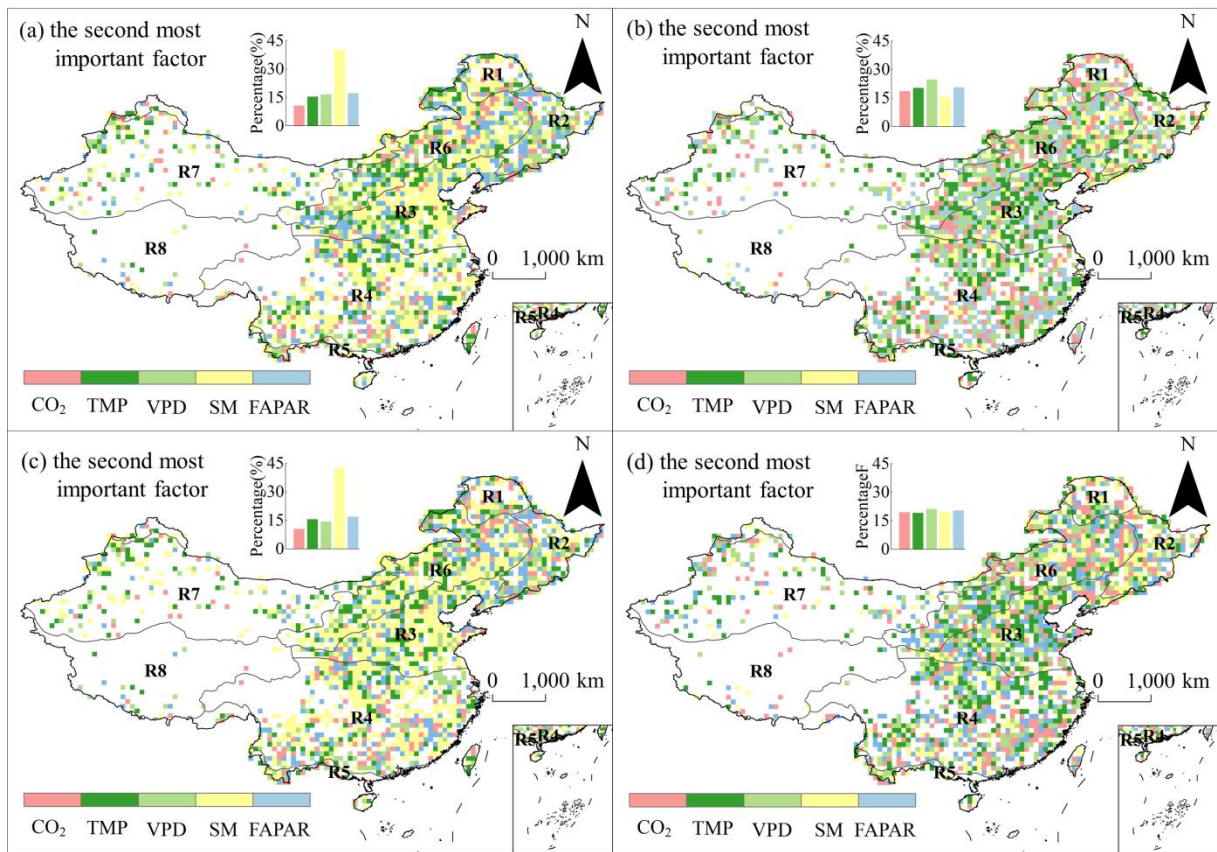


92

93 Fig. 11 Spatial distribution of trigger thresholds and dynamic characteristics for different GPP datasets

94 (a-b,d-e,h-i) trigger thresholds under different vegetation losses for GPPs, (c,f,g) graphs of dynamic

95 changes of trigger thresholds for  $GPP \leq GPP^{40th}$ .



96

97 Fig. 12 Random forest importance score with different SM datasets as input (a-b) the most and second most  
 98 important factor with GLDAS-SM, (c-d) largest and second largest important factor with ERA5-SM.

99 **5.4. Limitation**

100 It is worth noting that this study still has some limitations. We focused more on the  
 101 effects of drought on vegetation productivity. However, in addition to water stress, nutrient  
 102 limitation of nitrogen and phosphorus, insect pests, and forest fires may all have an impact on  
 103 change of thresholds. Furthermore, the independent contributions of the above-mentioned  
 104 influencing factors to changes in trigger threshold dynamics are not distinguished from a  
 105 quantitative perspective, which may blur the interactions between vegetation and drought.  
 106 Therefore, the process of influencing factors on carbon uptake in terrestrial ecosystems needs  
 107 to be subsequently studied in depth.

108 **6. Conclusion**

109 To investigate the response of vegetation health status to drought, we proposed a trigger  
110 threshold framework based on copula theory and conditional probability. Based on the  
111 quantification of vegetation vulnerability under different drought scenarios, drought trigger  
112 thresholds were estimated for different vegetation losses. In humid regions, GPP was  
113 positively correlated with SPEI, and response time of vegetation to drought was mostly based  
114 on short time scales (less than or equal to 4 months). Under the same GPP loss, the probability  
115 of vegetation loss increased with increasing drought intensity. In addition, the probability of  
116 substantial GPP loss was smaller under the same drought stress. It is found that the risk of  
117 vegetation productivity loss was significantly higher in eastern China than in western region,  
118 and that the drought trigger threshold was also higher in this region.

119 Analysis of the dynamics of the trigger thresholds through a 15-year moving window  
120 revealed a decreasing trend in northeast China (R1, R2, R6). In addition, similar conclusions  
121 were obtained from the analysis of trigger thresholds and dynamics for multiple GPP datasets.  
122 That is, the vegetation resistance gradually increased over time. In contrast, the R3 region,  
123 where water scarcity is a prominent issue, is vulnerable to lower levels of drought. Notably,  
124 based on the GLDAS\_SM and ERA5\_SM datasets, it is found that the dynamics of trigger  
125 thresholds were attributed to SM, while the interaction of CO<sub>2</sub> fertilization and other factors  
126 could mitigate the negative effects of water deficit on vegetation. It is expected that these  
127 findings will contribute to an improved understanding of vegetation loss under drought stress,  
128 leading to the development of timely and effective strategies  
129 to mitigate the impacts of drought on ecosystem health and thus improve resilience of  
130 terrestrial ecosystem.

## 131 **Acknowledgements**

132 This research was jointly supported by the National Natural Science Foundation of China  
133 (grant number 52279026), the National Key R&D Program of China (grant number  
134 2021YFC3000203), the Strategic Priority Research Program of the Chinese Academy of  
135 Sciences (grant number XDA28060100), and the Natural Science Foundation of Inner  
136 Mongolia Autonomous Region (grant number 2021ZD12).

## 137 **References**

- 138 Alsafadi, K., Alansari, N., Mokhtar, A. et al., 2022. An evapotranspiration deficit-based drought index to detect  
139 variability of terrestrial carbon productivity in the Middle East. *Environ. Res. Lett.*, 17(1): 014051.  
140 <https://doi.org/10.1088/1748-9326/ac4765>
- 141 Anderegg, W.R.L., Flint, A., Huang, C. et al., 2015. Tree mortality predicted from drought-induced vascular  
142 damage. *Nat. Geosci.*, 8(5): 367-371. <https://doi.org/10.1038/NGEO2400>
- 143 Breiman, L., 2001. Random forests. *Mach. Learn.*, 45(1): 5-32. <https://doi.org/10.1023/A:1010933404324>
- 144 Buttlar, J.v., Zscheichler, J., Rammig, A. et al., 2018. Impacts of droughts and extreme-temperature events on  
145 gross primary production and ecosystem respiration: a systematic assessment across ecosystems and  
146 climate zones. *Biogeosci. Discuss.*, 15(5): 1-39. <https://doi.org/10.5194/bg-2017-393>
- 147 Chen, C., Park, T., Wang, X. et al., 2019a. China and India lead in greening of the world through land-use  
148 management. *Nat. Sustain.*, 2(2): 122-129. <https://doi.org/10.1038/s41893-019-0220-7>
- 149 Chen, H., Bai, X., Li, Y. et al., 2021a. Soil drying weakens the positive effect of climate factors on global gross  
150 primary production. *Ecol. Indic.*, 129: 107953. <https://doi.org/10.1016/j.ecolind.2021.107953>
- 151 Chen, N., Song, C., Xu, X. et al., 2021b. Divergent impacts of atmospheric water demand on gross primary  
152 productivity in three typical ecosystems in China. *Agric. For. Meteorol.*, 307: 108527.

153 <https://doi.org/10.1016/j.agrformet.2021.108527>

154 Chen, W., Zhu, D., Huang, C. et al., 2019b. Negative extreme events in gross primary productivity and their  
155 drivers in China during the past three decades. *Agric. For. Meteorol.*, 275: 47-58.  
156 <https://doi.org/10.1016/j.agrformet.2019.05.002>

157 Choat, B., Brodribb, T.J., Brodersen, C.R. et al., 2018. Triggers of tree mortality under drought. *Nature*,  
158 558(7711): 531-539. <https://doi.org/10.1038/s41586-018-0240-x>

159 Ciais, P., Reichstein, M., Viovy, N. et al., 2005. Europe-wide reduction in primary productivity caused by the  
160 heat and drought in 2003. *Nature*, 437(7058): 529-533. <https://doi.org/10.1038/nature03972>

161 Delbart, N., Ciais, P., Chave, J. et al., 2010. Mortality as a key driver of the spatial distribution of aboveground  
162 biomass in Amazonian forest: results from a dynamic vegetation model. *Biogeosciences*, 7(10):  
163 3027-3039. <https://doi.org/10.5194/bg-7-3027-2010>

164 Deng, Y., Wang, X., Wang, K. et al., 2021. Responses of vegetation greenness and carbon cycle to extreme  
165 droughts in China. *Agric. For. Meteorol.*, 298-299: 108307.  
166 <https://doi.org/10.1016/j.agrformet.2020.108307>

167 Fan, K., Zhang, Q., Singh, V.P. et al., 2019. Spatiotemporal impact of soil moisture on air temperature across the  
168 Tibet Plateau. *Sci. Total Environ.*, 649: 1338-1348. <https://doi.org/10.1016/j.scitotenv.2018.08.399>

169 Fang, W., Huang, S., Huang, Q. et al., 2019. Bivariate probabilistic quantification of drought impacts on  
170 terrestrial vegetation dynamics in mainland China. *J. Hydrol.*, 577: 123980.  
171 <https://doi.org/10.1016/j.jhydrol.2019.123980>

172 Feng, S., Trnka, M., Hayes, M. et al., 2017. Why do different drought indices show distinct future drought risk  
173 outcomes in the U.S. Great Plains? *Journal of Climate*, 30(1): 265-278.  
174 <https://doi.org/10.1175/jcli-d-15-0590.1>

175 Gao, D., Wang, S., Li, Z. et al., 2021. Threshold of vapour–pressure deficit constraint on light use efficiency  
176 varied with soil water content. *Ecohydrology*. <https://doi.org/10.1002/eco.2305>

177 Gentine, P., Green, J.K., Guérin, M. et al., 2019. Coupling between the terrestrial carbon and water cycles—a  
178 review. *Environ. Res. Lett.*, 14(8). <https://doi.org/10.1088/1748-9326/ab22d6>

179 Green, J.K., Seneviratne, S.I., Berg, A.M. et al., 2019. Large influence of soil moisture on long-term terrestrial  
180 carbon uptake. *Nature*, 565(7740): 476-479. <https://doi.org/10.1038/s41586-018-0848-x>

181 Grossiord, C., Buckley, T.N., Cernusak, L.A. et al., 2020. Plant responses to rising vapor pressure deficit. *New*  
182 *Phytol.*, 226(6). <https://doi.org/10.1111/nph.16485>

183 Gu, H., Liu, Z., 2015. On the distribution, socio-economic impact and formation mechanism of agricultural  
184 drought disaster in Hunan. *Journal of Shanxi Agricultural University(Social Science Edition)*, 14(11):  
185 1081-1085.(in Chinese). <https://doi.org/10.13842/j.cnki.issn1671-816x.2015.11.002>

186 Guo, Y., Huang, S., Huang, Q. et al., 2020. Propagation thresholds of meteorological drought for triggering  
187 hydrological drought at various levels. *Sci. Total Environ.*, 712: 136502.  
188 <https://doi.org/10.1016/j.scitotenv.2020.136502>

189 Han, Z., Huang, S., Huang, Q. et al., 2021. GRACE-based high-resolution propagation threshold from  
190 meteorological to groundwater drought. *Agric. For. Meteorol.*, 307: 108476.  
191 <https://doi.org/10.1016/j.agrformet.2021.108476>

192 He, P., Ma, X., Han, Z. et al., 2022. Uncertainties of gross primary productivity of Chinese grasslands based on  
193 multi-source estimation. *Front. Environ. Sci.*, 10. <https://doi.org/10.3389/fenvs.2022.928351>

194 He, Q., Ju, W., Dai, S. et al., 2021. Drought risk of global terrestrial gross primary productivity over the last  
195 40 years detected by a remote sensing-driven process model. *J. Geophys. Res.-Biogeosci.*, 126(6).  
196 <https://doi.org/10.1029/2020jg005944>

197 He, W., Ju, W., Jiang, F. et al., 2020. Peak growing season patterns and climate extremes-driven responses of  
198 gross primary production estimated by satellite and process based models over North America. *Agric.  
199 For. Meteorol.*, 298-299: 108292. <https://doi.org/10.1016/j.agrformet.2020.108292>

200 Huang, L., He, B., Chen, A. et al., 2016. Drought dominates the interannual variability in global terrestrial net  
201 primary production by controlling semi-arid ecosystems. *Sci Rep*, 6(1): 24639.  
202 <https://doi.org/10.1038/srep24639>

203 Jha, S., Das, J., Sharma, A. et al., 2019. Probabilistic evaluation of vegetation drought likelihood and its  
204 implications to resilience across India. *Glob. Planet. Change*, 176: 23-35.  
205 <https://doi.org/10.1016/j.gloplacha.2019.01.014>

206 Jiang, H., Xu, X., Guan, M. et al., 2020. Determining the contributions of climate change and human activities to  
207 vegetation dynamics in agro-pastoral transitional zone of northern China from 2000 to 2015. *Sci. Total  
208 Environ.*, 718: 134871. <https://doi.org/10.1016/j.scitotenv.2019.134871>

209 Jiang, W., Wang, L., Zhang, M. et al., 2021. Analysis of drought events and their impacts on vegetation  
210 productivity based on the integrated surface drought index in the Hanjiang River Basin, China. *Atmos.  
211 Res.*, 254(1): 105536. <https://doi.org/10.1016/j.atmosres.2021.105536>

212 Jiao, W., Wang, L., McCabe, M.F., 2021. Multi-sensor remote sensing for drought characterization: current  
213 status, opportunities and a roadmap for the future. *Remote Sens. Environ.*, 256: 112313.  
214 <https://doi.org/10.1016/j.rse.2021.112313>

215 Joshi, J., Stocker, B., Hofhansl, F. et al., 2020. Towards a unified theory of plant photosynthesis and hydraulics.  
216 *BioRxiv*. <https://doi.org/10.1101/2020.12.17.423132>

217 Konings, A.G., Williams, A.P., Gentine, P., 2017. Sensitivity of grassland productivity to aridity controlled by  
218 stomatal and xylem regulation. *Nat. Geosci.*, 10(4): 284-288. <https://doi.org/10.1038/ngeo2903>

219 Korth, H., Tsyganenko, N.A., Johnson, C.L. et al., 2015. Modular model for Mercury's magnetospheric magnetic  
220 field confined within the average observed magnetopause. *J. Geophys. Res-Space Phys.*, 120(6):  
221 4503-4518. <https://doi.org/10.1002/2015JA021022>

222 Lai, C., Li, J., Wang, Z. et al., 2018. Drought-induced reduction in net primary productivity across mainland  
223 China from 1982 to 2015. *Remote Sens. Environ.*, 10(9): 1433. <https://doi.org/10.3390/rs10091433>

224 Li, C., Li, H., Li, J. et al., 2019a. Using NDVI percentiles to monitor real-time crop growth. *Comput. Electron.*  
225 *Agric.*, 162: 357-363. <https://doi.org/10.1016/j.compag.2019.04.026>

226 Li, J., Xushu, W., Wang, Z. et al., 2021. Changes of drought characteristics in future in Pearl River Basin  
227 describing by a new comprehensive standardized drought index. *Journal of Hydraulic Engineering*,  
228 52(04): 486-497.(in Chinese). <https://doi.org/10.13243/j.cnki.slxb.20200320>

229 Li, P., Huang, Q., Huang, S. et al., 2022a. Various maize yield losses and their dynamics triggered by drought  
230 thresholds based on Copula-Bayesian conditional probabilities. *Agric. Water Manag.*, 261.  
231 <https://doi.org/10.1016/j.agwat.2021.107391>

232 Li, X., Li, Y., Chen, A. et al., 2019b. The impact of the 2009/2010 drought on vegetation growth and terrestrial  
233 carbon balance in Southwest China. *Agric. For. Meteorol.*, 269-270: 239-248.  
234 <https://doi.org/10.1016/j.agrformet.2019.01.036>

235 Li, Y., Chen, Y., Li, Z., 2019c. Dry/wet pattern changes in global dryland areas over the past six decades. *Glob.*  
236 *Planet. Change*, 178: 184-192. <https://doi.org/10.1016/j.gloplacha.2019.04.017>

237 Li, Y., Huang, S., Wang, H. et al., 2022b. High-resolution propagation time from meteorological to agricultural  
238 drought at multiple levels and spatiotemporal scales. *Agric. Water Manag.*, 262.  
239 <https://doi.org/10.1016/j.agwat.2021.107428>

240 Liu, J.F., Arend, M., Yang, W.J. et al., 2017. Effects of drought on leaf carbon source and growth of European

241 beech are modulated by soil type. *Sci Rep*, 7: 42462. <https://doi.org/10.1038/srep42462>

242 Liu, L., Gudmundsson, L., Hauser, M. et al., 2020. Soil moisture dominates dryness stress on ecosystem  
243 production globally. *Nat. Commun.*, 11(1): 4892. <https://doi.org/10.1038/s41467-020-18631-1>

244 Liu, L., Peng, S., AghaKouchak, A. et al., 2018. Broad consistency between satellite and vegetation model  
245 estimates of net primary productivity across global and regional scales. *J. Geophys. Res.-Biogeosci.*,  
246 123(12): 3603-3616. <https://doi.org/10.1029/2018jg004760>

247 Liu, Y., Zhou, Y., Ju, W. et al., 2014. Impacts of droughts on carbon sequestration by China's terrestrial  
248 ecosystems from 2000 to 2011. *Biogeosciences*, 11(10): 2583-2599.  
249 <https://doi.org/10.5194/bg-11-2583-2014>

250 Ma, M., Yuan, W., Dong, J. et al., 2018. Large-scale estimates of gross primary production on the Qinghai-Tibet  
251 plateau based on remote sensing data. *Int. J. Digit. Earth*, 11(11): 1166-1183.  
252 <https://doi.org/10.1080/17538947.2017.1381192>

253 Ma, X., Huete, A., Moran, S. et al., 2015. Abrupt shifts in phenology and vegetation productivity under climate  
254 extremes. *J. Geophys. Res.-Biogeosci.*, 120(10): 2036-2052. <https://doi.org/10.1002/2015JG003144>

255 Madakumbura, G.D., Goulden, M.L., Hall, A. et al., 2020. Recent California tree mortality portends future  
256 increase in drought-driven forest die-off. *Environ. Res. Lett.*, 15(12): 124040.  
257 <https://doi.org/10.1088/1748-9326/abc719>

258 Mahecha, M.D., Bastos, A., Bohn, F.J. et al., 2022. Biodiversity loss and climate extremes — study the  
259 feedbacks. *Nature*, 612: 30-32. <https://doi.org/10.1038/d41586-022-04152-y>

260 McDowell, N.G., Allen, C.D., Marshall, L., 2010. Growth, carbon-isotope discrimination, and drought-associated  
261 mortality across a *Pinus ponderosa* elevational transect. *Glob. Change Biol.*, 16(1): 399-415.  
262 <https://doi.org/10.1111/j.1365-2486.2009.01994.x>

263 Piao, S., Liu, Z., Wang, T. et al., 2017. Weakening temperature control on the interannual variations of spring  
264 carbon uptake across northern lands. *Nat. Clim. Chang.*, 7(5). <https://doi.org/10.1038/nclimate3277>

265 Piao, S., Wang, X., Park, T. et al., 2019. Characteristics, drivers and feedbacks of global greening. *Nature*  
266 reviews. *Earth & environment*, 1(1): 14-27. <https://doi.org/10.1038/s43017-019-0001-x>

267 Poulter, B., Frank, D., Ciais, P. et al., 2014. Contribution of semi-arid ecosystems to interannual variability of the  
268 global carbon cycle. *Nature*, 509(7502): 600-3. <https://doi.org/10.1038/nature13376>

269 Qu, Y., Lv, J., Zhang, W. et al., 2018. Progress in research on historical extreme drought in China. *Adv. Water*  
270 *Sci.*, 29(02): 283-292.(in Chinese). <https://doi.org/10.14042/j.cnki.32.1309.2018.02.016>

271 Reichstein, M., Tenhunen, J.D., Rouspard, O. et al., 2002. Severe drought effects on ecosystem CO<sub>2</sub> and H<sub>2</sub>O  
272 fluxes at three Mediterranean evergreen sites: revision of current hypotheses? . *Glob. Change Biol.*,  
273 8(10): 999-1017. <https://doi.org/10.1046/j.1365-2486.2002.00530.x>

274 Ruppert, J.C., Harmony, K., Henkin, Z. et al., 2015. Quantifying drylands' drought resistance and recovery: the  
275 importance of drought intensity, dominant life history and grazing regime. *Glob. Change Biol.*, 21(3):  
276 1258-1270. <https://doi.org/10.1111/gcb.12777>

277 Saleska S R, Didan K, Huete A R et al., 2007. Amazon Forests Green-Up During 2005 Drought. *Science*,  
278 318(5850): 612. <https://doi.org/10.1126/science.1146663>

279 Shi, X., Chen, C., Shang, Y. et al., 2020. Analysis of correlation between vegetation net primary productivity and  
280 drought in Huai River Basin. *Jiangsu Agricultural Sciences* 48(03): 255-261. (in Chinese).  
281 <https://doi.org/10.15889/j.issn.1002-1302.2020.03.046>

282 Sklar, A., 1959. *Fonctions de Repartition an Dimensions et Leurs Marges*. *Publ.inst.statist.univ.paris*.

283 Su, J., Wen, M., Ding, Y. et al., 2016. Hiatus of global warming:a review. *Chinese Journal of Atmospheric*  
284 *Sciences*, 40(06): 1143-1153. (in Chinese). <https://doi.org/10.3878/j.issn.1006-9895.1512.15242>

285 Su, Y., Guo, B., Zhou, Z. et al., 2020. Spatio-temporal variations in groundwater revealed by GRACE and its  
286 driving factors in the Huang-Huai-Hai Plain, China. *Sensors*, 20(3): 922.  
287 <https://doi.org/10.3390/s20030922>

288 Sun, B., Zhao, H., Wang, X., 2016. Effects of drought on net primary productivity: roles of temperature, drought  
289 intensity, and duration. *Chin. Geogr. Sci.*, 26(2): 270-282. <https://doi.org/10.1007/s11769-016-0804-3>

290 Sun, Z., Long, D., Yang, W. et al., 2020. Reconstruction of GRACE data on changes in total water storage over  
291 the global land surface and 60 basins. *Water Resour. Res.*, 56(4): e2019WR026250.  
292 <https://doi.org/10.1029/2019wr026250>

293 Tagesson, T., Schurgers, G., Horion, S. et al., 2020. Recent divergence in the contributions of tropical and boreal  
294 forests to the terrestrial carbon sink. *Nat. Ecol. Evol.*, 4(2): 202-209.  
295 <https://doi.org/10.1038/s41559-019-1090-0>

296 Vicente-Serrano, S.M., Beguería, S., López-Moreno, J.I., 2010. A multiscalar drought index sensitive to global  
297 warming: the standardized precipitation evapotranspiration index. *Journal of Climate*, 23(7): 1696-1718.  
298 <https://doi.org/10.1175/2009jcli2909.1>

299 Vicente-Serrano, S.M., Gouveia, C., Camarero, J.J. et al., 2013. Response of vegetation to drought time-scales  
300 across global land biomes. *Proc. Natl. Acad. Sci.*, 110(1): 52-7.  
301 <https://doi.org/10.1073/pnas.1207068110>

302 Wang, S., Zhang, Y., Ju, W. et al., 2021. Tracking the seasonal and inter-annual variations of global gross  
303 primary production during last four decades using satellite near-infrared reflectance data *Sci. Total*  
304 *Environ.*, 755: 142569. <https://doi.org/10.1016/j.scitotenv.2020.142569>

305 Wei, X., He, W., Zhou, Y. et al., 2022. Global assessment of lagged and cumulative effects of drought on  
306 grassland gross primary production. *Ecol. Indic.*, 136. <https://doi.org/10.1016/j.ecolind.2022.108646>

307 Wu, J., Jing, Y., Guan, D. et al., 2013. Controls of evapotranspiration during the short dry season in a temperate  
308 mixed forest in Northeast China. *Ecohydrology*, 6(5): 775-782. <https://doi.org/10.1002/eco.1299>

309 Wu, X., Jiang, D., 2022. Probabilistic impacts of compound dry and hot events on global gross primary  
310 production. *Environ. Res. Lett.*, 17(3): 034049. <https://doi.org/10.1088/1748-9326/ac4c5b>

311 Xiao, J., Chevallier, F., Gomez, C. et al., 2019. Remote sensing of the terrestrial carbon cycle: a review of  
312 advances over 50 years. *Remote Sens. Environ.*, 233: 111383. <https://doi.org/10.1016/j.rse.2019.111383>

313 Xu, C., McDowell, N.G., Fisher, R.A. et al., 2019a. Increasing impacts of extreme droughts on vegetation  
314 productivity under climate change. *Nat. Clim. Chang.*, 9(12): 948-953.  
315 <https://doi.org/10.1038/s41558-019-0630-6>

316 Xu, H., Zhao, C., Wang, X., 2019b. Spatiotemporal differentiation of the terrestrial gross primary production  
317 response to climate constraints in a dryland mountain ecosystem of northwestern China. *Agric. For.  
318 Meteorol.*, 276: 107628. <https://doi.org/10.1016/j.agrformet.2019.107628>

319 Yan, Z., Liu, D., Jia, X. et al., 2021. Maize tassel development, physiological traits and yield under heat and  
320 drought stress during flowering stage. *Sci. Agric. Sin.*, 54(17): 3592-3608.(in Chinese).  
321 <https://doi.org/10.3864/j.issn.0578-1752.2021.17.004>

322 Yang, Y., Guan, H., Batelaan, O. et al., 2016. Contrasting responses of water use efficiency to drought across  
323 global terrestrial ecosystems. *Sci Rep*, 6(1): 1-8. <https://doi.org/10.1038/srep23284>

324 Yang, Y., Mao, K., Han, X. et al., 2018. Characteristics of drought disaster and its impact on grain production in  
325 China from 1949 to 2016. *China Agricultural Informatics*, 30(05): 76-90.(in Chinese).  
326 <https://doi.org/10.12105/j.issn.1672-0423.20180509>.

327 Yang, Y., Roderick, M.L., Zhang, S. et al., 2019. Hydrologic implications of vegetation response to elevated CO<sub>2</sub>  
328 in climate projections. *Nat. Clim. Chang.*, 9(1): 44-48. <https://doi.org/10.1038/s41558-018-0361-0>

- 329 Yao, N., Li, Y., Dong, Q.g. et al., 2020. Influence of the accuracy of reference crop evapotranspiration on  
330 drought monitoring using standardized precipitation evapotranspiration index in mainland China. *Land*  
331 *Degrad. Dev.*, 31(2): 266-282. <https://doi.org/10.1002/ldr.3447>
- 332 Yu, Z., Wang, J., Liu, S. et al., 2017. Global gross primary productivity and water use efficiency changes under  
333 drought stress. *Environ. Res. Lett.*, 12(1): 014016. <https://doi.org/10.1088/1748-9326/aa5258>
- 334 Yuan, M., Zhu, Q., Zhang, J. et al., 2021. Global response of terrestrial gross primary productivity to climate  
335 extremes. *Sci. Total Environ.*, 750: 142337. <https://doi.org/10.1016/j.scitotenv.2020.142337>
- 336 Yuan, W., Cai, W., Chen, Y. et al., 2016. Severe summer heatwave and drought strongly reduced carbon uptake  
337 in Southern China. *Sci Rep*, 6(1): 1-12 <https://doi.org/10.1038/srep18813>
- 338 Yue, S., Sheng, X., Yang, F., 2022. Spatiotemporal evolution and meteorological triggering conditions of  
339 hydrological drought in the Hun River basin, NE China. *Nat. Hazards Earth Syst. Sci.*, 22(3): 995-1014.  
340 <https://doi.org/10.5194/nhess-22-995-2022>
- 341 Zeiter, M., Schärer, S., Zweifel, R. et al., 2016. Timing of extreme drought modifies reproductive output in  
342 semi-natural grassland. *J. Veg. Sci.*, 27(2): 238-248. <https://doi.org/10.1111/jvs.12362>
- 343 Zhang, A., Jia, G., Ustin, S.L., 2021. Water availability surpasses warmth in controlling global vegetation trends  
344 in recent decade: revealed by satellite time series. *Environ. Res. Lett.*, 16(7): 074028.  
345 <https://doi.org/10.1088/1748-9326/ac0b68>
- 346 Zhang, L., Wang, L., Zhang, X. et al., 2014. The basic principle of random forest and its applications in ecology:  
347 a case study of *Pinus yunnanensis*. *Acta Ecologica Sinica*, 34(03): 650-659.(in Chinese).  
348 <https://doi.org/10.5846/stxb201306031292>
- 349 Zhang, L., Xiao, J., Li, J. et al., 2012. The 2010 spring drought reduced primary productivity in southwestern  
350 China. *Environ. Res. Lett.*, 7(4): 045706. <https://doi.org/10.1088/1748-9326/7/4/045706>

351 Zhang, M., Yuan, X., Otkin, J.A. et al., 2022a. Climate warming outweighs vegetation greening in intensifying  
352 flash droughts over China. *Environ. Res. Lett.*, 17(5): 054041.  
353 <https://doi.org/10.1088/1748-9326/ac69fb>

354 Zhang, q., Yao, Y., Li, Y. et al., 2020. Progress and prospect on the study of causes and variation regularity of  
355 droughts in China. *Acta Meteorol. Sin.*, 78(03): 500-521.(in Chinese).  
356 <https://doi.org/10.11676/qxxb2020.032>

357 Zhang, Q., Yuan, R., Singh, V.P. et al., 2022b. Dynamic vulnerability of ecological systems to climate changes  
358 across the Qinghai-Tibet Plateau, China. *Ecol. Indic.*, 134: 108483.  
359 <https://doi.org/10.1016/j.ecolind.2021.108483>

360 Zhang, X., Yamaguchi, Y., 2014. Characterization and evaluation of MODIS-derived drought severity index  
361 (DSI) for monitoring the 2009/2010 drought over southwestern China. *Nat. Hazards*, 74(3): 2129-2145.  
362 <https://doi.org/10.1007/s11069-014-1278-1>

363 Zhang, X., Zhang, Y., Tian, J. et al., 2022c. CO<sub>2</sub> fertilization is spatially distinct from stomatal conductance  
364 reduction in controlling ecosystem water-use efficiency increase. *Environ. Res. Lett.*, 17(5): 054048.  
365 <https://doi.org/10.1088/1748-9326/ac6c9c>

366 Zhao, M., Running, S.W., 2010. Drought-induced reduction in global terrestrial net primary production from  
367 2000 through 2009. *Science*, 329(5994): 940-943. <https://doi.org/10.1126/science.1192666>

368 Zheng, F., Ciais, P., Bastos, A. et al., 2020. Sensitivity of gross primary productivity to climatic drivers during  
369 the summer drought of 2018 in Europe. *Philos. Trans. R. Soc. B-Biol. Sci.*, 375(1810): 20190747.  
370 <https://doi.org/10.1098/rstb.2019.0747>

371 Zheng, X., Huang, S., Peng, J. et al., 2022. Flash droughts identification based on an improved framework and  
372 their contrasting impacts on vegetation over the Loess Plateau, China. *Water Resour. Res.*, 58,

373 e2021WR031464. <https://doi.org/10.1029/2021WR031464>

374 Zhou, S., Zhang, Y., Park Williams, A.P. et al., 2019. Projected increases in intensity, frequency, and terrestrial  
375 carbon costs of compound drought and aridity events. *Sci. Adv.*, 5(1): eaau5740.  
376 <https://doi.org/10.1126/sciadv.aau5740>

377 Zhu, X., Xin, Y., Ge, H., 2015. Recursive random forests enable better predictive performance and model  
378 interpretation than variable selection by LASSO. *J. Chem Inf. Model.*, 55(4): 736-746.  
379 <https://doi.org/10.1021/ci500715e>

380 Zscheischler, J., Mahecha, M.D., Buttlar, J.v. et al., 2014a. A few extreme events dominate global interannual  
381 variability in gross primary production. *Environ. Res. Lett.*, 9(3): 035001.  
382 <https://doi.org/10.1088/1748-9326/9/3/035001>

383 Zscheischler, J., Michalak, A.M., Schwalm, C. et al., 2014b. Impact of large-scale climate extremes on  
384 biospheric carbon fluxes: an intercomparison based on MsTMIP data *Glob. Biogeochem. Cycle*, 28(6):  
385 585-600. <https://doi.org/10.1002/2014GB004826>

386 Zscheischler, J., Seneviratne, S.I., 2017. Dependence of drivers affects risks associated with compound events.  
387 *Sci. Adv.*, 3(6): e1700263. <https://doi.org/10.1126/sciadv.1700263>

388